Asociación Argentina
de Mecánica Computacional

Mecánica Computacional Vol XXIX, págs. 2255-2266 (artículo completo)
Eduardo Dvorkin, Marcela Goldschmit, Mario Storti (Eds.)
Buenos Aires, Argentina, 15-18 Noviembre 2010

TWO-DIMENSINONAL SIMULATION OF THE WENNER METHOD WITH THE BOUNDARY ELEMENT METHOD – INFLUENCE OF THE LAYERING DISCRETIZATION

Rodrigo Dias[a], Simone dos S. Hoefel[b], Edmundo G. de A. Costa[a], José A. M. Carrer[c], and Luiz A. de Lacerda[b]

[a]*Department of Civil Engineering, COPPE – Federal University of Rio de Janeiro, CEP 21945-970, Rio de Janeiro, RJ, Brazil,* rodrigodias@coc.ufrj.br,edmundo_costa@coc.ufrj.br, http://www.coc.ufrj.br/

[b]*Department of Structures, LACTEC – Institute of Technology for Development, CEP 81531-980, Curitiba, PR, Brazil,* shoefel@gmail.com, alkimin@lactec.org.br, http://www.lactec.org.br/pt/

[c]*Department of Mathematics, – Federal University of Paraná, Curitiba, PR, Brazil,* carrer@mat.ufpr.br, http://www.ufpr.br/portal/

Keywords: Boundary Element Method, Wenner Method, Resistivity.

Abstract. This work presents a two-dimensional boundary element formulation for the analysis of electrical potential distribution in layered soils. The analyses are focused on the simulation of the Wenner method, which is widely used for the identification of the resistivity profile of soils. This problem involves current injection and retrieval from source and sinks points, respectively, while measuring potential values in other two electrodes, with varying spacing among them. Two-dimensional (2D) analyses are limited for obtaining the resistivity profile, but can provide an interesting insight to the studied problem. Sub-regions are employed to model each layer in the varying resistivity profile. The profiles used in this work are continuous curves adapted from practical experiment results. The influence of the number of adopted layers in the numerical potential values is evaluated and the quality of the numerical results is assessed for the different types of profiles.

Copyright © 2010 Asociación Argentina de Mecánica Computacional http://www.amcaonline.org.ar

1 INTRODUCTION

The soil resistivity and its stratification are of extreme importance for dimensioning electrical equipment protection systems. It is known that the resistance of a grounding grid is directly proportional to the resistivity (ρ) of the soil on which it sits (Visacro, 2002). So, when seeking a low resistance grounding, it is necessary to have a well based knowledge of the soil´s layers resistivity profile. (Zeng et al., 2000).

A soil in its true form (a half-space) can have its resistivity to vary in every direction, in others words, anisotropic. One of the ways to address this issue in a simple solution is to use the use if the process of layer into stratification and applying the governing equation system for each layer, separately, with the proper resistivity to every one of them. There are many factors that have influence over the soil resistance (Kindermann et al. 1995). The Wenner method (Wenner, 1916) is a common technique used in soil resistance determination. The resistivity profile overlap is made using the group of measuring results and mathematical expressions developed from the three-dimensional fundamental solution for an infinite half-space.

In the last few years, several authors have been using the boundary elements technique for solving potential distribution problems (Wrobel and Aliabadi, 2002), such as cathodic protection problems (Yan, 1992; Brichau, 1994; Lacerda et al., 2006), which require the knowledge of the medium resistivity.

This work presents a 2D boundary element formulation for the analysis of electrical potential distribution in layered soils. The analyses are focused on the simulation of the Wenner method, which is widely used for the identification of the resistivity profile of soils. The Wenner configuration consists of aligning four electrodes in the soil with constant spacing, using the two extreme electrodes for the injection and withdrawal of the electric current and measuring the potential difference between the intermediary electrodes. The analyses are limited on a 2D case for obtaining a resistivity profile, however, it can provide and interesting insight to the studied problem. The numerical method provides a great versatility to the analysis, due to the possibility of including in the measuring scenario diverse conditions, such as: juxtaposed sub-regions, parallel, or not, to the free surface, among others. Here, sub-regions are used to simulate the varying soil resistivity profile. The resistivity profiles analyzed in this article are continuous curves, adopted results from practical field experiments. The influence of the number of layers on the central electrodes potential difference with the varying spacing is evaluated.

The implemented formulation forms a specific computational environment (in development) for this kind of analyses, aiming for soil resistivity evaluation.

2 GOVERNING EQUATIONS

Consider the problem of electrical potential distribution in a bi-dimensional layered soil domain $\Omega = \Omega_1 \cup \Omega_2 ... \cup \Omega_n$ and $\Omega_i \cap \Omega_{i+1} = \emptyset$ of infinity extent along the *z* direction, with different boundary conditions, as shown in Figure 1.

Copyright © 2010 Asociación Argentina de Mecánica Computacional http://www.amcaonline.org.ar

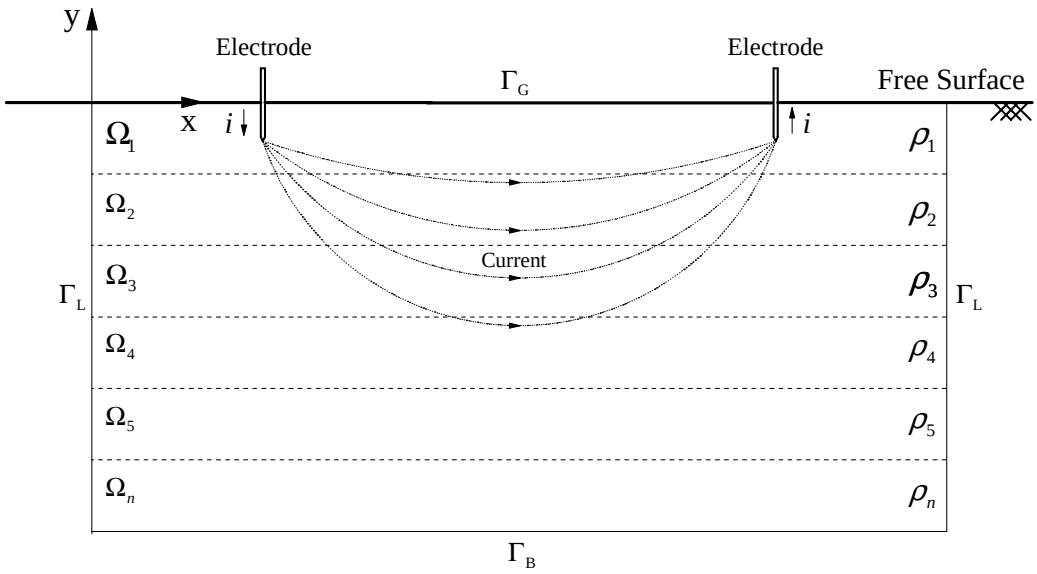

Figure 1: Geometry of the problem.

In these conditions, the governing Poisson equation may be applied and can be written as

$$\nabla.(k\nabla\phi(\mathbf{x})) = -\sum_{l=1}^{NS} Q_l \delta(\xi_l^f, \xi), \quad \text{in region } \Omega \tag{1}$$

where NS is the number of sources in the domain; $\phi(\mathbf{x})$ is the electric potential; Q_l is the intensity of the existing source ξ_l^f located at $(x_{\xi_l^f}, y_{\xi_l^f})$; ξ is a domain point located at (x_ξ, y_ξ); $\delta(\xi_l^f, \xi)$ is the Dirac delta generalized function and $k = 1/\rho$ is the conductivity in the medium.

The described problem is subjected to the following boundary conditions: Dirichlet condition, $\phi(\mathbf{x}) = 0$, in the boundary Γ_B (bottom) and in the boundary Γ_L (sides), Neumann condition, $i(\mathbf{x}) = k\dfrac{\partial\phi}{\partial \mathrm{n}}(\mathbf{x}) = 0$, only in the boundary of the plane free surface Γ_G (ground), where $\mathbf{x}$ is the field point located at (x, y) and n is the unit outward normal vector.

3 NUMERICAL FORMULATION

3.1 Classical Boundary Element Method

According to Green's second identify, (Eq. (1)) can be transformed into the following boundary integral equation

$$c(\xi)\phi(\xi) = \int_\Gamma \phi^*(\xi, \mathbf{x}) i(\mathbf{x}) d\Gamma - \int_\Gamma i^*(\xi, \mathbf{x})\phi(\mathbf{x}) d\Gamma + \sum_{l=1}^{NS} Q_l \phi^*(\xi_l^f, \xi) \tag{2}$$

where Γ is equal to $\Gamma = \Gamma_G \cup \Gamma_L \cup \Gamma_B$; $\phi^*(\xi, \mathbf{x})$ and $i^*(\xi, \mathbf{x})$ are the electrical potential and current density fundamental solutions, respectively; the coefficient $c(\xi)$ is dependent on the geometry at the source point ξ; $\phi(\mathbf{x})$ and $i(\mathbf{x})$ are the electrical potential and current density at the boundary Γ. The fundamental solution expressions are given by

Copyright © 2010 Asociación Argentina de Mecánica Computacional http://www.amcaonline.org.ar

$$\phi^*(\xi,\mathbf{x}) = \frac{1}{2k\pi}\ln\left(\frac{1}{r}\right) \tag{3}$$

and

$$i^*(\xi,\mathbf{x}) = -\frac{1}{2\pi r}\frac{\partial r}{\partial n} \tag{4}$$

where r is the distance between the source point ξ and the field point $\mathbf{x}$.

The boundary element method may be used to solve (Eq. (2)) requiring discretization of all surfaces, if appropriate fundamental solutions are not used. However, the previously described problem can be solved with Green's functions that satisfy specific boundary conditions allowing the reduction of boundary discretization. The following integral equations refer to the specific geometry which combines several sub-regions with one of them including the two sources and the flat free surface ground, as shown in Figure 2.

The BEM model used in this work makes use of the Green's function that satisfy the boundary condition in the free surface ground, thus, requiring only the discretization of the boundaries of the bottom, sides and interfaces. Two models are used: a) single domain model with three different discretizations, which is used to evaluate the proper element size for the analyses (Figure 2 (a) and (b)) multi-domain model with sub-domain discretizations varying from 1 to 6 (Figure 2b).

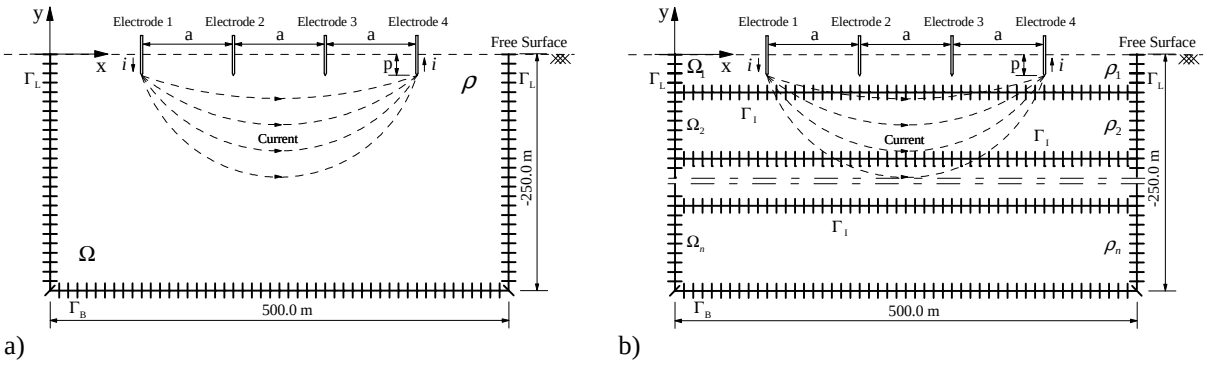

Figure 2: Geometry of the BEM models: (a) Model 1 and (b) Model 2.

In the first model, two unit loads of same magnitude, but opposite signs, are in the domain. Introducing the appropriate boundary conditions at the discretized bottom Γ_B and sides Γ_L, into Eq. (2) and assuming NE constant elements with linear geometry, and applying the collocation method to the integral equation the following equation may be obtained

$$c(\xi_p)\phi(\xi_q) = \sum_{q=1}^{NE}\int_{-1}^{1}\phi_{fs}^*(\xi_p,\mathbf{x}_q)i(\mathbf{x}_q)\left|J\right|d\eta + \sum_{l=1}^{NS}Q_l\phi_{fs}^*(\xi_l^f,\xi_q) \tag{5}$$

where ξ_q refers to the functional node p with p ranging from 1 to NE; $\left|J\right|$ is the Jacobian; $i(\mathbf{x}_q)$ is the unknown current density at point boundary element $\mathbf{x}_q$; $\phi_{fs}^*(\xi_p,\mathbf{x}_q)$ is the Green's function that satisfy the boundary condition at the free surface ground at the boundary element $\mathbf{x}_q$, and whose details are given in a subsequent section; $\phi_{fs}^*(\xi_l^f,\xi_q)$ is the incident field regarding the electrical potential generated by the real source.

The second model differs only by the presence of the sub-regions. Introducing the

Copyright © 2010 Asociación Argentina de Mecánica Computacional http://www.amcaonline.org.ar

appropriate boundary conditions at the discretized interfaces Γ_I (where continuity of electrical potentials and equilibrium of the current densities must exist) into Eq. (2), the following equation may be obtained:

- Region (Ω_1)

$$c(\xi_p)\phi(\xi_q) = \sum_{q=1}^{NE}\int_{-1}^{1}\phi_{fs}^{*}(\xi_p,\mathbf{x}_q)i(\mathbf{x}_q)\left|J\right|d\eta - \sum_{q=1}^{NE}\int_{-1}^{1}i_{fs}^{*}(\xi_p,\mathbf{x}_q)\phi(\mathbf{x}_q)\left|J\right|d\eta + \sum_{l=1}^{NS}Q_l\phi_{fs}^{*}(\xi_l^f,\xi_q) \tag{6}$$

- Regions ($\Omega_2,\ \Omega_3,\cdots,\Omega_n$)

$$c(\xi_p)\phi(\xi_q) = \sum_{q=1}^{NE}\int_{-1}^{1}\phi^{*}(\xi_p,\mathbf{x}_q)i(\mathbf{x}_q)\left|J\right|d\eta - \sum_{q=1}^{NE}\int_{-1}^{1}i^{*}(\xi_p,\mathbf{x}_q)\phi(\mathbf{x}_q)\left|J\right|d\eta \tag{7}$$

After assembling and solving the system of equations, it is possible to obtain the nodal values of the electrical potentials and current densities at all elements. The potential at any point of the domain can then be calculated by applying the boundary integral equation.

4 GREEN'S FUNCTION

4.1 Image Source Method

By applying the image source method one obtains a Green's function, which directly satisfies the boundary condition at the free surface, reducing the discretization of the problem.

In the present article, this Green's function is defined as $\phi_{fs}^{*}(\xi,\mathbf{x})$ and is given by

$$\phi_{fs}^{*}(\xi,\mathbf{x}) = \frac{1}{2k\pi}\left[\ln\left(\frac{1}{r}\right)+\ln\left(\frac{1}{r'}\right)\right] \tag{8}$$

and its normal derivative is given by

$$i_{fs}^{*}(\xi,\mathbf{x}) = -\frac{1}{2\pi}\left[\frac{1}{r}\frac{\partial r}{\partial n}+\frac{1}{r'}\frac{\partial r'}{\partial n}\right] \tag{9}$$

where r is the distance from the source to the field point and r' is the distance from the image of the source to the field point.

5 NUMERICAL RESULTS

5.1 Wenner method

The Wenner configuration is a commonly used technique for determining the resistivity of the soil profiles. The Wenner configuration consists of four electrodes inserted in the soil, usually cylindrical with same length L and diameter d, equally spaced by a distance a and aligned in a certain direction as shown in Figure 2.

In practice, it is observed that as the spacing between the rods increases, so does the depth of investigation. Figure 3 illustrates how the flow of electric current behaves in the soil,

Copyright © 2010 Asociación Argentina de Mecánica Computacional http://www.amcaonline.org.ar

depending on the resistivity of the layers.

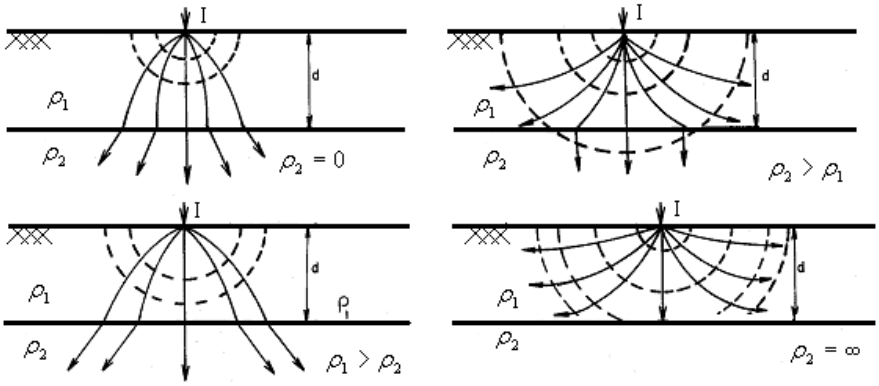

Figure 3: Behavior of electrical current depending on the soil resistivity in the case of two layers. Adapted from (Kindermann et al. 1995).

The equation that allows us to determine the potential at a point p any, away from the point q of injection of an electric current, in a three-dimensional (3D) half-space is given by (Kindermann et al. 1995)

$$\Phi_p(r \mid r') = \frac{\rho I}{4\pi r_q} + \frac{\rho I'}{4\pi r'_q} \tag{10}$$

Applying the Wenner method, the potential difference between the central rods is given by

$$\Phi_{23} = \frac{\rho I}{4\pi}\left(\frac{1}{a} + \frac{2}{\sqrt{a^2 + (2p)^2}} - \frac{2}{\sqrt{(2a)^2 + (2p)^2}}\right) \tag{11}$$

The resistivity is given by

$$\rho = \frac{4\pi a R}{\left(1 + \frac{2a}{\sqrt{a^2 + (2p)^2}} - \frac{2a}{\sqrt{(2a)^2 + (2p)^2}}\right)} \tag{12}$$

Where R is the resistance of the soil, which is given by $R = \frac{\Phi_{23}}{I}\left(\frac{V}{A} = \Omega\right)$, a is the spacing between the rods and p is the depth of the rods. For large spacing between the rods $a > 20p$, the following equation can be adopted

$$\rho = 2\pi a R \tag{13}$$

It is important to note that Φ_{23} decays in inverse proportion to the spacing (a^{-1}). In an analogous analysis, but using the 2D fundamental solution (Eq. (8)) the potential at some point between the two points of injection and withdrawal of electric current behaves according to Figure 4 and is given by

Copyright © 2010 Asociación Argentina de Mecánica Computacional http://www.amcaonline.org.ar

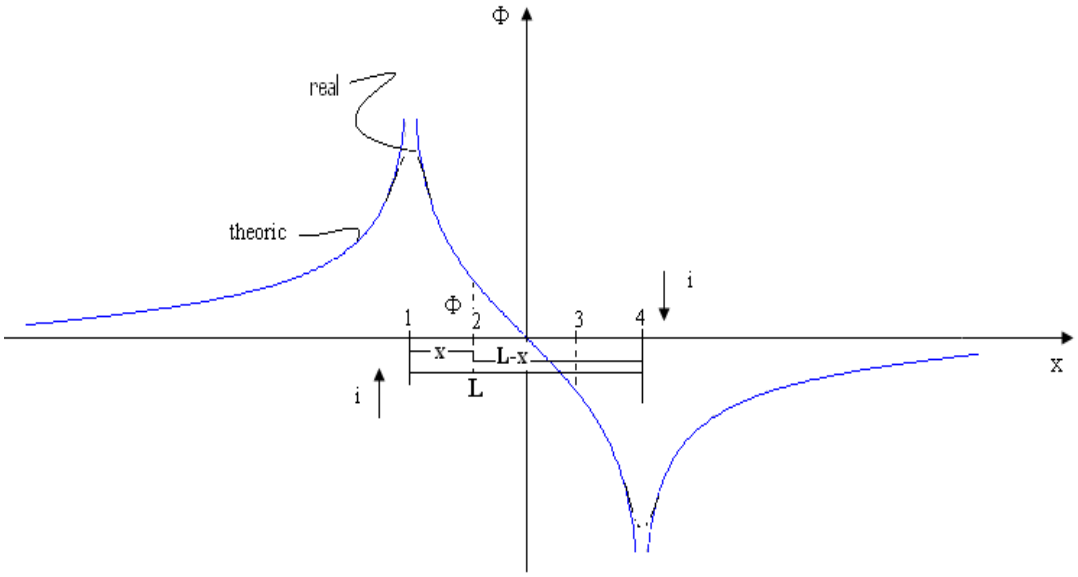

Figure 4: Lines of theoretical and real potential for the case with points of injection and withdrawal of electrical currents in the ground.

$$\Phi_x^{(1)} = \frac{\rho I/d}{2\pi} \ln\left(\frac{1}{x}\right) \tag{14}$$

and

$$\Phi_{L-x}^{(4)} = -\frac{\rho I/d}{2\pi} \ln\left(\frac{1}{L-x}\right) \qquad where \;\; L = \overline{12} \tag{15}$$

Thus

$$\Phi_{23} = \Phi_x^{(1)} - \Phi_{L-x}^{(4)} = \frac{\rho I/d}{2\pi}\left(\ln\left(\frac{1}{x}\right) - \ln\left(\frac{1}{L-x}\right)\right) \tag{16}$$

Analyzing Figure 4 we can show the following results

$$\begin{array}{lll} x \to 0 & \Phi \to +\infty & in \;\; 1 \\ x \to \dfrac{L}{2} & \Phi \to 0 & in \;\; medium \;\; point \\ x \to L & \Phi \to -\infty & in \;\; 2 \end{array} \tag{17}$$

The Wenner configuration in the 2D case gives the following potential values at the central electrodes

$$\Phi_2(\xi, X) = \frac{\rho I/d}{\pi}\left(\ln(2) + \frac{1}{2}\left(\ln\left((2a)^2 + (2p)^2\right) - \ln\left(a^2 + (2p)^2\right)\right)\right) \tag{18}$$

Copyright © 2010 Asociación Argentina de Mecánica Computacional http://www.amcaonline.org.ar

$$\Phi_3(\xi, X) = \frac{\rho I/d}{\pi}\left(-\ln(2) + \frac{1}{2}\left(\ln\left(a^2 + (2p)^2\right) - \ln\left((2a)^2 + (2p)^2\right)\right)\right) \tag{19}$$

Which results in

$$\Phi_{23}(\xi, X) = \frac{\rho I/d}{\pi}\left(\ln(2)\right) \tag{20}$$

Isolating the resistivity in Eq. (14), one arrives at the following equation

$$\rho = \frac{\pi R}{\ln(2)} \tag{21}$$

This constant behavior of the potential difference in the 2D case is curious, but can be verified through a limiting analysis of the superposition of two infinite series of electric sources and sinks (Dias 2009).

5.2 Numerical simulations

In the numerical analyses two resistivity profiles were adopted, obtained from experimental field tests - Example 3.5.1 and 3.9.1 of the Kindermann et al. (1995). These profiles are show in Figure 5.

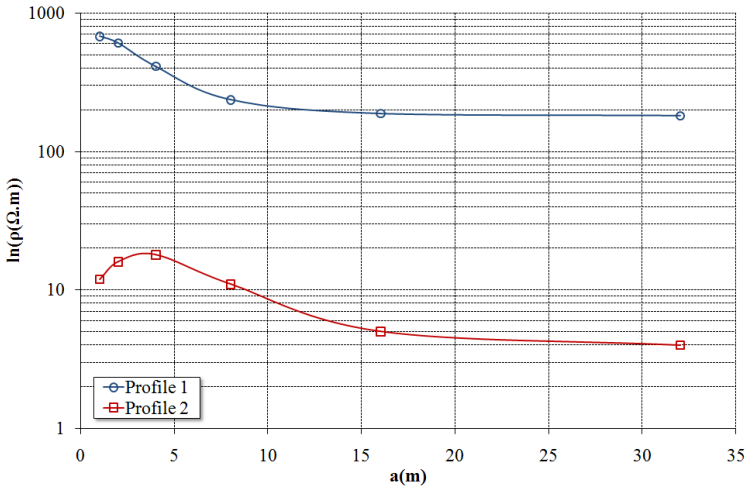

Figure 5: Resistive profiles adopted for the analyses.

The profiles were simulated with average resistivity values for each sub-domain, according to the adopted domain discretization. These values are presented in the tables 1 and 2, one for each profile.

Discretization 1		Discretization 2		Discretization 3	
ρ (Ohm.m)	Layer (m)	ρ (Ohm.m)	Layer (m)	ρ (Ohm.m)	Layer (m)
386,3	0 a 250	684,0	0 a 1	684,0	0 a 1
		326,8	1 a 250	611,0	1 a 2
				255,8	2 a 250

a)

Copyright © 2010 Asociación Argentina de Mecánica Computacional http://www.amcaonline.org.ar

Discretization 4		Discretization 5		Discretization 6	
ρ (Ohm.m)	**Layer (m)**	**ρ (Ohm.m)**	**Layer (m)**	**ρ (Ohm.m)**	**Layer (m)**
684,0	0 a 1	684,0	0 a 1	684,0	0 a 1
611,0	1 a 2	611,0	1 a 2	611,0	1 a 2
415,0	2 a 4	415,0	2 a 4	415,0	2 a 4
202,7	4 a 250	237,0	4 a 8	237,0	4 a 8
		185,5	8 a 250	189,0	8 a 16
				182,0	16 a 250

b)

Table 1: Resistivity profile 1 adapted to the analysis: (a) discretization 1 to 3; (b) discretization 4 to 6.

Discretization 1		Discretization 2		Discretization 3	
ρ (Ohm.m)	**Layer (m)**	**ρ (Ohm.m)**	**Layer (m)**	**ρ (Ohm.m)**	**Layer (m)**
11,0	0 a 250	12,0	0 a 1	12,0	0 a 1
		10,8	1 a 250	16,0	1 a 2
				9,5	2 a 250

a)

Discretization 4		Discretization 5		Discretization 6	
ρ (Ohm.m)	**Layer (m)**	**ρ (Ohm.m)**	**Layer (m)**	**ρ (Ohm.m)**	**Layer (m)**
12,0	0 a 1	12,0	0 a 1	12,0	0 a 1
16,0	1 a 2	16,0	1 a 2	16,0	1 a 2
18,0	2 a 4	18,0	2 a 4	18,0	2 a 4
6,7	4 a 250	11,0	4 a 8	11,0	4 a 8
		4,5	8 a 250	5,0	8 a 16
				4,0	16 a 250

b)

Table 2: Resistivity profile 2 adapted to the analysis: (a) discretization 1 to 3; (b) discretization 4 to 6.

Aiming to evaluate the influence of the convergence of the discretization method, we adopt a mesh A with 179 elements a mesh B with 501 elements and a mesh C with 1000 elements for the single domain region, the same way we adopt a mesh A with 1181 elements a mesh B 1740 elements a mesh C with 2001 elements for the case with two sub-regions. The remaining domain were used a single mesh for each domain with 2183, 3185, 2883 and 4167 elements for the cases with 3, 4, 5, 6 sub-regions respectively. Considering that for the case with one and two sub-regions were adopted with few meshes and meshes with many elements that we observed no major changes in numerical results. The results obtained with the BEM approach from the data specified above for one and two sub-regions for the profiles 1 and 2 are shown in Figures 6 and (a) and (b) are show the relative errors for the cases with the meshes A, B and C, and in the Figures 7 (a) and (b) the cases with 3, 4, 5 and 6 sub-regions respectively shown

Copyright © 2010 Asociación Argentina de Mecánica Computacional http://www.amcaonline.org.ar

the potential difference between the rods 2 and 3.

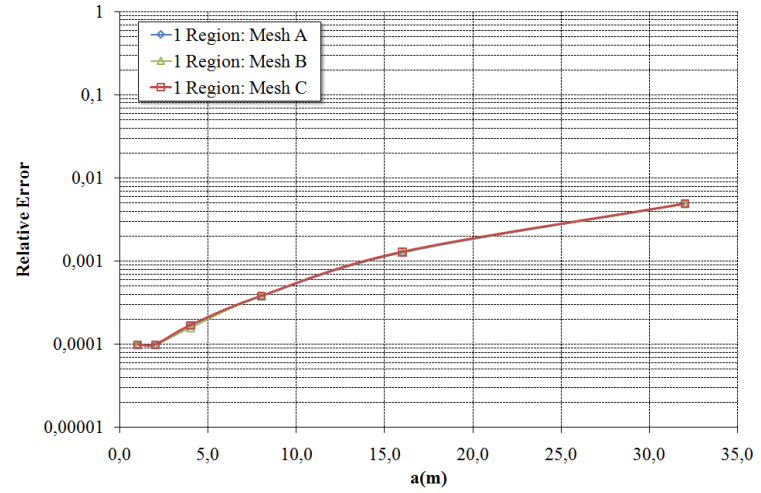

a)

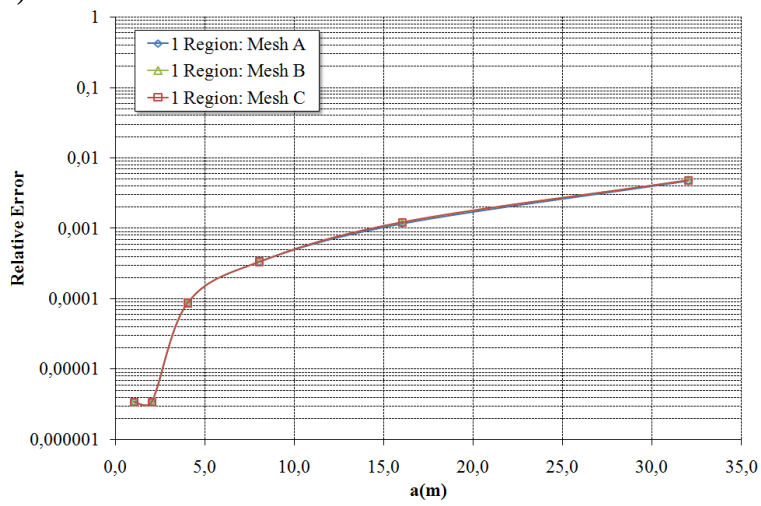

b)

Figure 6: Relative errors in logarithmic scale versus rod spacing obtained using the mesh A, mesh B and mesh C to the two profiles adopted solution: a) Profile 1, with one and two sub-regions; b) Profile 2, with one and two sub-regions.

Due to potential difference via the Wenner method for the 2D case be constant, it was observed that with only two layers in the laminate, reached convergence for the cases analyzed. As shown in Figure 6 (a) and (b), both for the first profile how to profile the second domain with two sub-regions already gives us a relative error of about 4.97×10^{-6} that are practically the same order of magnitude of errors obtained for cases with 3, 4, 5 and 6 sub-regions. How we view Figure 7 (a) and (b) the potential are practically identical. Thus it is not necessary with the use of domains 3, 4, 5 and 6 sub-regions for the case analyzed in 2D. Unlike what is observed in the 3D case that in most cases the discretization in layers is necessary.

Copyright © 2010 Asociación Argentina de Mecánica Computacional http://www.amcaonline.org.ar

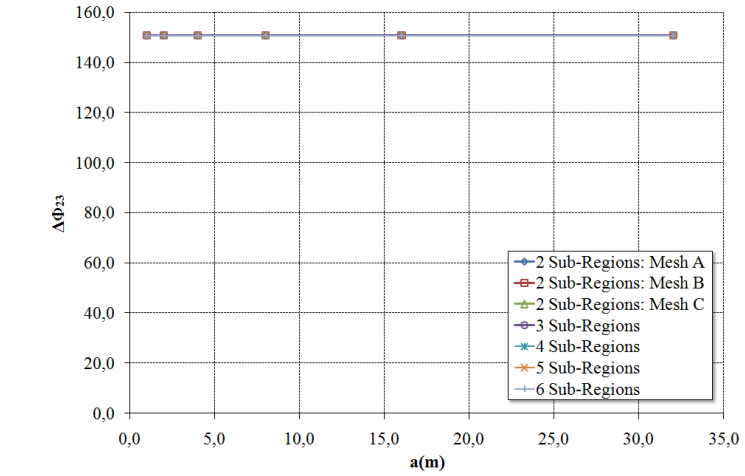

a)

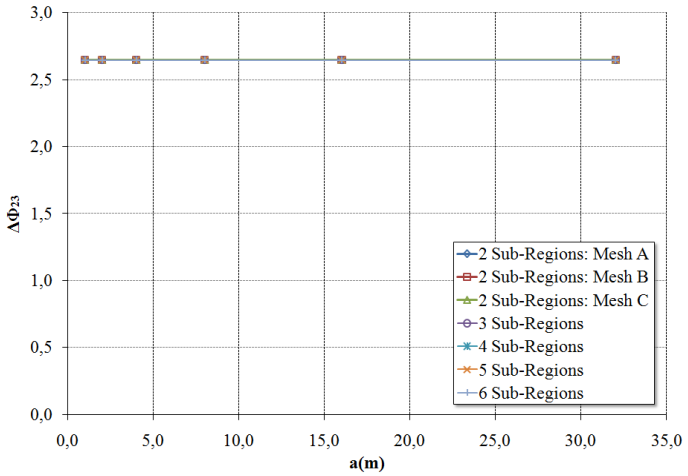

b)

Figure 7: The potential difference between the intermediary electrodes versus rod spacing obtained to cases with 3, 4, 5 and 6 sub-regions: a) Profile 1 to 3, 4 5 and 6 sub-regions; b) Profile 2, with 3, 4, 5 and 6 sub-regions.

As seen in Figure 6 (a) and (b) for profiles 1 and 2 the relative error for the case with a sub-region has been increasing as the spacing each junior rods have been increasing. Usually in practice, the 3D case it is observed that as we increase the spacing between the stems the error tends to decrease because the current lines reach higher depths. This error analysis to the problem is due to having just one region and due to the fact that we have adopted an average resistivity in that region.

6 CONCLUSIONS

The analysis developed in this work shows that for the resistivity profiles analyzed, we do not need more than two layers in case of 2D to achieve good results with the BEM approach that is in agreement with the analytical response obtained for the problem. The results obtained with the 2D BEM formulation are in agreement with the theoretical responses obtained for the problem and contributes to the understanding of the phenomenon for future 3D formulations already in early stages of development. The case analyzed 2D does not allow us to compare the result with the real 3D case.

Copyright © 2010 Asociación Argentina de Mecánica Computacional http://www.amcaonline.org.ar

ACKNOWLEDGEMENTS

We would like to thank *Conselho Nacional de Desenvolvimento Científico e Tecnológico* (CNPq) of Brazil for financial support. (Processo 558696/2008-2), and CAPES (Coordenação de Aperfeiçoamento de Pessoal de Nível Superior).

REFERENCES

Brichau, F. A. Mathematical Model for the Cathodic Protection of Underground Pipelines Including Stray Currents. *Vrije Universiteit, Brussel,* 1994.

Capalli, A. Aterramento Elétrico. *Saber Eletrônica, São Paulo,* n.329, p.56-9, 2000.

Colominas, I.; Navarrina, F., and Casteleiro, M. A Boundary Element Formulation for the Substation Grounding design. *E.T.S. de Ingenieros de Caminos, Canales y Puertos. Dpto. de Métodos Matemáticos y Representación Universidad de La Coruña*, Spain; 1998.

Dias, R., Lacerda, L. A., and Carrer, J.A.M. Simulação do Método de Wenner para Determinação da Resistividade de Solos com o Método dos Elementos de Contorno. *Cilamce* 2008.

Dias, R., Formulação Bidimensional do Método dos Elementos de Contorno Para Problemas de Potencial elétrico em Meios Estratificados. *Dissertação de Mestrado, Universidade Federal do Paraná* 2009.

Fernandes C.E. de M. Fundamentos de Prospecção Geofisica, *Editora Interciência, Rio de Janeiro,* 1984.

Lacerda, L.A., Silva, J.M., and Lázaris, J.L. Dual Boundary Element Formulation For Half-space Cathodic Protection Analysis, *Engineering Analysis with Boundary Elements*, v.31, p.559 - 567, 2007.

NBR 5410 /1997. Instalações Elétricas de Baixa Tensão. *Associação Brasileira de Normas Técnicas*, 1997.

Kindermann, G.; Campagnolo, J. M., Aterramento Elétrico. *Sagra-DCLuzzato, 3ª Edição, Porto Alegre*, 214pp, 1995.

Visacro S.F., Aterramentos Elétricos: Conceitos Básico, Técnicas de Medição e Instrumentação, Filosofias de Aterramento, *Artlibe, São Paulo*, 2002

Wenner F.A., Method of Measuring Earth Resistivity, Bulletin of the National Bureau of Standards, Washington D.C., vol. 12, 1916.

Wrobel L.C., and Aliabadi. M.H., The Boundary Element Method, *Wiley, Chichester, London,* 2002.

Yan, J.F., Pakalapati, S.N.R., Nguyen, T.V., and Whiter. E. Mathematical Modeling of Cathodic Protection Using The Boundary Element Method with a Nonlinear Polarization Curve, *Department of Chemical Engineering, Texas A&M University, College Station, Texas* 77843-3122, 1992.

Zeng R., Jinliang, H.E., Wang, Z., Yanqing, G.A.O., Sun, W., Su, Q., Analysis on Influence of Long Vertical Grounding Electrodes on Grounding System for Substation, *IEEE, Beijing, China*, 2000.

Copyright © 2010 Asociación Argentina de Mecánica Computacional http://www.amcaonline.org.ar